A neutron scattering study of hydrogen dynamics in coarse-grained and nanostructured $ZrCr_2H_3$

2011 J. Phys.: Condens. Matter 23 065402

(http://iopscience.iop.org/0953-8984/23/6/065402)

J. Phys.: Condens. Matter **23** (2011) 065402 (8pp) doi:10.1088/0953-8984/23/6/065402

A neutron scattering study of hydrogen dynamics in coarse-grained and nanostructured $ZrCr_2H_3$

A V Skripov[1], T J Udovic[2], J J Rush[2,3] and M A Uimin[1]

[1] Institute of Metal Physics, Urals Branch of the Academy of Sciences, Ekaterinburg 620041, Russia
[2] NIST Center for Neutron Research, National Institute of Standards and Technology, Gaithersburg, MD 20899-6102, USA
[3] Department of Materials Science and Engineering, University of Maryland, College Park, MD 20742-2115, USA

Received 12 November 2010, in final form 27 December 2010
Published 25 January 2011
Online at stacks.iop.org/JPhysCM/23/065402

Abstract
The vibrational spectra of hydrogen and parameters of H diffusion in the coarse-grained C15-type system $ZrCr_2H_3$ and in nanostructured $ZrCr_2H_3$ have been studied by means of inelastic and quasielastic neutron scattering. It is found that the diffusive motion of hydrogen in coarse-grained $ZrCr_2H_3$ can be described in terms of at least two jump processes: a fast localized H motion with the jump rate τ_1^{-1} over the hexagons formed by interstitial Zr_2Cr_2 sites and a slower process with the rate τ_d^{-1} associated with H jumps leading to long-range diffusion. While $\tau_d^{-1}(T)$ in the range 250–380 K follows the Arrhenius law with the activation energy of 142 ± 4 meV, the temperature dependence of τ_1^{-1} deviates from Arrhenius behavior. The nanostructured $ZrCr_2H_3$ samples prepared by ball milling consist of C15-type grains and strongly distorted (amorphous-like) regions. H atoms in the strongly distorted regions are found to be immobile on the time scale of our experiments. The microscopic picture of H jump motion in the C15-type grains of the nanostructured samples is similar to that in coarse-grained $ZrCr_2H_3$; however, the ball milling leads to a considerable decrease in the jump rate τ_d^{-1}.

1. Introduction

Nanostructured metal–hydrogen systems have received much recent attention, mainly due to their potential for hydrogen storage applications. Such systems may also serve as model objects for studies of atomic diffusion in inhomogeneous media. It has been found that, for a number of nanostructured hydrides, the hydrogen absorption and desorption are significantly faster than in their coarse-grained counterparts [1–4]. However, little is known about the mechanisms responsible for the changes in hydrogen reaction kinetics. Microscopic information on the H jump motion in metal–hydrogen systems can be obtained from nuclear magnetic resonance (NMR) [5] and quasielastic neutron scattering (QENS) [6, 7] measurements. While NMR measurements of nuclear spin relaxation times can probe H jump rates over the frequency range of $\sim 10^4$–10^{10} s^{-1}, QENS measurements are sensitive to both the frequency (10^8–10^{12} s^{-1}) and the spatial scales of H jump motion. In the present work, quasielastic neutron scattering is applied to study the mechanisms and parameters of hydrogen diffusion in the coarse-grained cubic intermetallic hydride $ZrCr_2H_3$ and in nanostructured $ZrCr_2H_3$ hydrides prepared by ball milling.

The Laves-phase intermetallic compound $ZrCr_2$ can exist in either the hexagonal (C14-type) or the cubic (C15-type) structural modifications, both of which are known to absorb large amounts of hydrogen (up to ~4 H atoms per formula unit) [8–12]. According to neutron diffraction measurements [9–11], H atoms in C15-type $ZrCr_2H_x$ with $x < 3.1$ occupy only the tetrahedral g sites with $[Zr_2Cr_2]$ coordination; at higher x, a small fraction of H atoms start to fill the tetrahedral e sites with $[ZrCr_3]$ coordination. The cubic $ZrCr_2H_x$ system with $x \leqslant 0.5$ shows the highest H diffusivity [13] at $T < 200$ K among all the intermetallic hydrides studied. One of the interesting features of hydrogen diffusion in Laves-phase compounds is the coexistence of two frequency scales of H jump motion [14–19]. In most of the cubic Laves phases studied where H atoms occupy only

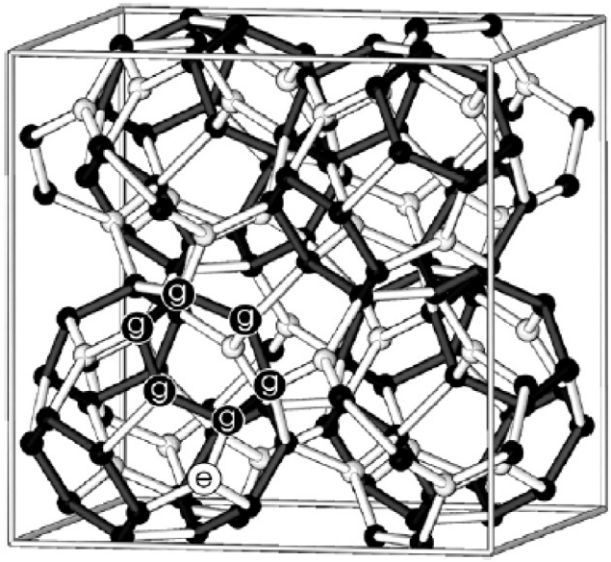

Figure 1. The spatial arrangement of interstitial g sites (dark spheres) and e sites (light spheres) in the cubic C15-type lattice.

interstitial sites of g type, the faster jump process corresponds to *localized* H motion within the hexagons formed by g sites (see figure 1), and the slower process (leading to long-range diffusion) is associated with H jumps from one g site hexagon to another. The difference between the characteristic rates of these jump processes is believed to result from the difference between the g–g distances r_1 (within the hexagon) and r_2 (between the nearest hexagons) [17, 19]. The results of the previous QENS study of cubic $ZrCr_2H_{0.45}$ [20] were consistent with two coexisting H jump processes. It should be noted, however, that the measurements [20] employed the neutron backscattering technique [6, 7] having a very narrow range of neutron energy transfer (or, in other words, a very narrow frequency 'window'). Because of this feature, only one of the two H jump processes could be probed at a given temperature; therefore, the H jump rates of the two processes in $ZrCr_2H_{0.45}$ were measured [20] in different temperature ranges. In the present work, we apply the time-of-flight QENS technique [6, 7] having a wide range of energy transfer to study H jump motion in cubic $ZrCr_2H_x$ with high hydrogen concentration. This gives us an opportunity to probe the two jump processes in the same temperature range.

The first x-ray diffraction study of the effects of ball milling in $ZrCr_2H_3$ [21] has revealed that the milling leads to the formation of strongly distorted (amorphous-like) regions coexisting with the cubic C15-type phase. The fraction of these amorphous-like regions is found to increase with increasing milling time. According to proton NMR measurements [21], the mobility of H atoms in the amorphous-like regions is much lower than in the C15-type phase. However, since the two H jump processes in C15-type $ZrCr_2H_x$ are not resolved by NMR [21–23], these measurements cannot give information on the effects of ball milling on the microscopic picture of H motion in the C15-type phase. One of the aims of the present work is to reveal such effects of ball milling using the QENS technique. This is the first study of the microscopic picture of H jump motion in a nanostructured Laves-phase hydride. QENS experiments are complemented by inelastic neutron scattering (INS) studies of the vibrational spectra of hydrogen in coarse-grained and ball-milled $ZrCr_2H_3$. Neutron vibrational spectroscopy allows us to probe the changes in the local environment of H atoms resulting from the ball milling.

2. Experimental details

The preparation of the samples was analogous to that described in [21]. The starting material for preparation of all the samples was powdered $ZrCr_2H_{0.5}$ with the cubic C15-type host-metal structure and the lattice parameter $a = 7.278$ Å. The coarse-grained (cg) sample of $ZrCr_2H_3$ was prepared by removing hydrogen from $ZrCr_2H_{0.5}$ at high temperature (750 °C) and rehydrogenating it to the desired H content in a Sieverts-type vacuum system. The amount of absorbed hydrogen (3.0 ± 0.1 H atoms per formula unit of $ZrCr_2$) was determined from the H_2 pressure change in the calibrated volume of the system. In the following, this sample will be denoted as cg-$ZrCr_2H_3$. Its lattice parameter ($a = 7.599$ Å) is in reasonable agreement with the literature data [9, 11] for $ZrCr_2H_x$ with $x \approx 3$. In order to prepare nanostructured samples, $ZrCr_2H_{0.5}$ powder was placed together with brass balls (powder to ball mass ratio 1:140) into a brass vial. The vial was evacuated and subsequently filled with H_2 gas at a pressure of 110 kPa. The mechanical milling was performed at room temperature using a vibrating ball mill for periods t_m of 1 and 3 h. In the process of milling, the samples absorbed hydrogen, and, for both values of t_m, the final amount of absorbed hydrogen (estimated from the H_2 pressure change in the vial) was approximately three H atoms per formula unit of $ZrCr_2$. In the following, the ball-milled (bm) samples with $t_m = 1$ and 3 h will be denoted as bm-$ZrCr_2H_3$ (1 h) and bm-$ZrCr_2H_3$ (3 h). For both ball-milled samples, x-ray diffraction patterns were similar to those reported in [21]. These patterns consist of the broadened Bragg peaks belonging to the C15-type structure and a very broad amorphous-like feature. The lattice parameters of the C15-type phase ($a = 7.608$ Å for $t_m = 1$ h and $a = 7.64$ Å for $t_m = 3$ h) are close to those found for coarse-grained $ZrCr_2H_x$ with $x \approx 3$ [9, 11]. The average grain size estimated from the broadening of the peaks belonging to the C15-type phase is 20 nm for $t_m = 1$ h and ~10 nm for $t_m = 3$ h.

All neutron scattering experiments were performed at the NIST Center for Neutron Research (Gaithersburg, Maryland, USA). Inelastic neutron scattering measurements of the hydrogen vibrational spectra at 4 K were made on the filter–analyzer neutron spectrometer (FANS) [24] using the Cu(220) monochromator and horizontal collimations of 20 min of arc before and after the monochromator. The measured range of neutron energy loss was 40–210 meV, and the energy resolution was about 4%–5% of the energy transfer. Quasielastic neutron scattering measurements were performed on a disk-chopper time-of-flight spectrometer (DCS) [25] and on a Fermi-chopper time-of-flight spectrometer (FCS) [26]. For the cg-$ZrCr_2H_3$, the temperature dependence of the QENS spectra $S_{exp}(Q, \omega)$ (where $\hbar\omega$ is the energy transfer and $\hbar Q$ is the elastic momentum transfer) was measured in

the range 200–380 K using DCS with the incident neutron wavelength $\lambda = 5.0$ Å. For this configuration, the energy resolution was 105 μeV (full width at half-maximum), and the Q range studied was 0.54–2.1 Å^{-1}. For the ball-milled $ZrCr_2H_3$ samples, the temperature dependence of $S_{exp}(Q, \omega)$ was studied in the range 204–375 K using FCS with $\lambda = 4.8$ Å. For this configuration, the energy resolution was 145 μeV, and the Q range probed was 0.54–2.41 Å^{-1}. At two temperatures ($T = 325$ and 375 K), QENS spectra for bm-$ZrCr_2H_3$ (3 h) were also measured using FCS with $\lambda = 6.0$ Å; these measurements provided better energy resolution (65 μeV) at the expense of a smaller Q range. The powdered samples were studied in hollow-cylinder Al containers, the sample thickness being 0.3 mm. The sample thickness was chosen to ensure ~90% neutron transmission and thus minimize multiple-scattering effects. For data analysis, the detectors were binned into nine groups. The scattering angles corresponding to the Bragg reflections were excluded from the analysis. The instrumental resolution functions were determined from the measured QENS spectra of the corresponding $ZrCr_2H_3$ samples at low temperatures (15 K for DCS and 4 K for FCS).

3. Results and discussion

3.1. Neutron vibrational spectroscopy

The experimental INS spectra for the cg- and bm-$ZrCr_2H_3$ samples are shown in figure 2. For the cg-$ZrCr_2H_3$, the shape of the INS spectrum resembles the corresponding shapes found for cubic $ZrCr_2H_x$ with lower hydrogen concentrations ($x = 0.9$ [27] and $x = 0.2$ and 0.5 [28]). However, the spectrum for $x = 3$ is shifted to somewhat lower $\hbar\omega$ values, as compared to the spectra for low-x samples. For example, the onset of the sharp rise in the scattered neutron intensity for cg-$ZrCr_2H_3$ is observed at ~110 meV (figure 2), while for $ZrCr_2H_{0.5}$ a similar rise starts at ~128 meV [28]. This shift may be related to the lattice expansion at higher H concentrations. The spectral features for cg-$ZrCr_2H_3$ are also broader than for the low-x $ZrCr_2H_x$ samples. In fact, for $ZrCr_2H_x$ with $x = 0.2$ and 0.5, the main peak in the INS spectrum at low temperature is split into two well-resolved peaks of nearly equal intensity [28]. The simplest approach to the description of INS spectra due to localized hydrogen vibrations is based on the model of a three-dimensional Einstein oscillator [29, 30]. For the $\hbar\omega$ range of fundamental modes, this model predicts three peaks of nearly equal intensity. Depending on the point symmetry of H sites, all or two of these peaks may be degenerate. For hydrogen at g sites of the C15-type lattice, we expect three non-degenerate peaks, since the point symmetry (m) of these sites is lower than axial. General features of the experimental INS spectrum for cg-$ZrCr_2H_3$ can be ascribed to H atoms at g sites (two unresolved peaks in the range 110–145 meV and a third peak in the range 145–170 meV). It is natural to attribute the broadening of the spectral features for cg-$ZrCr_2H_3$ to the dispersion of the corresponding bands due to H–H interactions.

As can be seen from figure 2, the behavior of the INS spectra in the range 40–100 meV for the ball-milled samples differs markedly from that for coarse-grained $ZrCr_2H_3$. While

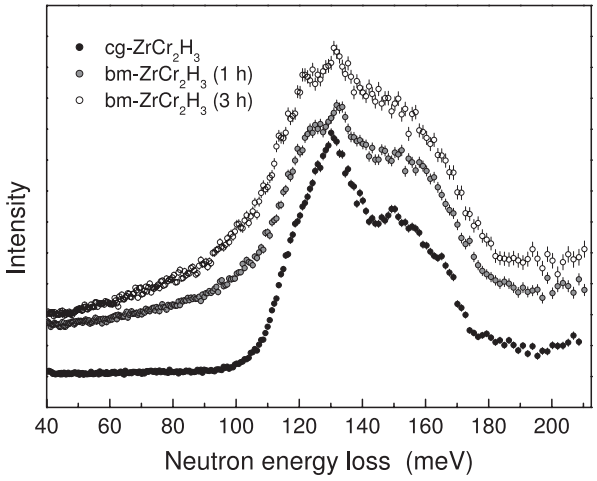

Figure 2. The low-temperature inelastic neutron scattering spectra for the cg- and bm-$ZrCr_2H_3$ samples. Vertical error bars correspond to one standard deviation.

for cg-$ZrCr_2H_3$, the spectrum shows just a flat background in this range, for the ball-milled samples, the scattered neutron intensity substantially increases with increasing energy transfer. The appearance of such a broad feature in the spectra for the ball-milled samples indicates a wide distribution of local environments of H atoms; it can be attributed to vibrations of H atoms in the regions with a strongly distorted lattice (these regions are also responsible for the 'amorphous-like' features in x-ray diffraction patterns). Note that the relative intensity of the broad feature in the range 40–100 meV increases with increasing milling time. The shape of the spectra in the range 110–170 meV for the ball-milled samples resembles that for cg-$ZrCr_2H_3$. Therefore, the corresponding spectral features can be ascribed to H atoms in a slightly distorted C15-type phase.

3.2. Quasielastic neutron scattering spectra

QENS spectra for cg-$ZrCr_2H_3$ measured at $T = 200$ and 225 K can be satisfactorily described by a sum of two components: an 'elastic' line represented by the spectrometer resolution function $R(Q, \omega)$ and a resolution-broadened Lorentzian 'quasielastic' line. The relative intensity of the quasielastic component is found to increase with increasing Q, its half-width being nearly independent of Q. However, at higher temperatures ($T \geqslant 250$ K), the description in terms of a sum of an elastic line and a single Lorentzian quasielastic component leads to systematic deviations of the model QENS spectra from the experimental ones. For these temperatures, a better description of the experimental data can be achieved if a second Lorentzian quasielastic component is added to the model spectra, so the experimental scattering function $S_{exp}(Q, \omega)$ is fitted with the incoherent scattering function

$$S_{inc}(Q, \omega) = A_0(Q)\delta(\omega) + A_1(Q)L(\omega, \Gamma_1) + A_2(Q)L(\omega, \Gamma_2) \quad (1)$$

convoluted with $R(Q, \omega)$. Here, $\delta(\omega)$ is the elastic δ-function, $L(\omega, \Gamma_i)$ are the Lorentzian functions with the half-widths

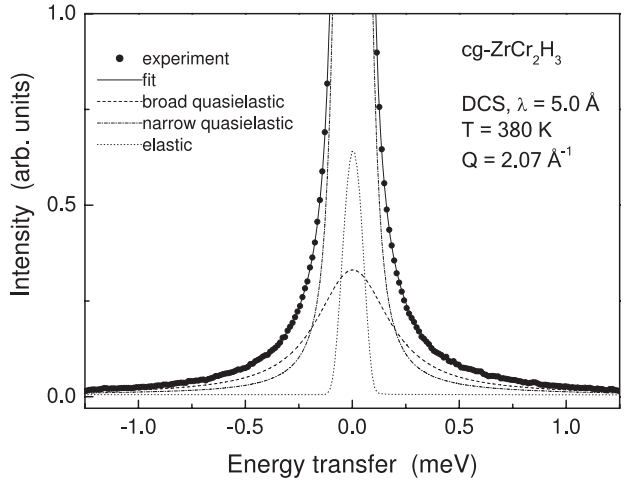

Figure 3. The QENS spectrum for cg-$ZrCr_2H_3$ measured at $T = 380$ K and $Q = 2.07$ Å^{-1}. The circles are the experimental points interpolated to the uniform energy grid. The full curve shows the fit of the three-component model (equation (1)) to the data. The dotted line represents the elastic component (the spectrometer resolution function), and the broken curves show two Lorentzian quasielastic components.

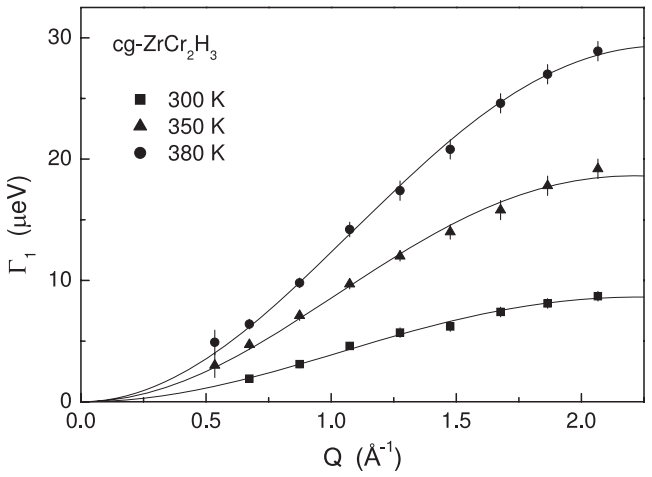

Figure 4. The half-width at half-maximum (HWHM) of the narrow Lorentzian QENS component for cg-$ZrCr_2H_3$ as a function of Q at $T = 300$, 350, and 380 K. The full curves show the fits of the Chudley–Elliott model (equation (2)) to the data.

Γ_i, and $A_0 + A_1 + A_2 = 1$. As an example of the data, figure 3 shows the QENS spectrum of cg-$ZrCr_2H_3$ measured on DCS at $T = 380$ K and $Q = 2.07$ Å^{-1}. At the first stage of the analysis, we have used the model scattering function (equation (1)) with two amplitudes (A_0, A_1, with $A_2 = 1 - A_0 - A_1$) and two half-widths (Γ_1, Γ_2) which are independent fit parameters. At all the temperatures studied, the intensity of the broader quasielastic component, $A_2(Q)$, is found to increase with increasing Q, and its half-width Γ_2 appears to be nearly independent of Q. Since these features are typical of a spatially confined atomic motion [6, 7], the broad quasielastic component is attributed to a fast localized H motion with the jump rate τ_1^{-1}. In this case, the value of Γ_2 should be proportional to τ_1^{-1}, while the Q dependence of A_2 should be related to the geometry of this motion.

The half-width of the narrow quasielastic component, Γ_1, is found to increase with increasing Q, showing signs of saturation near $Q \approx 2$ Å^{-1}. Furthermore, the values of Γ_1 rapidly increase with increasing temperature. These features suggest that the narrow quasielastic component originates from a jump process leading to long-range H diffusion. The intensity of the elastic component, A_0, for cg-$ZrCr_2H_3$ is found to be small (about 7% of the total scattered intensity) and nearly independent of Q and T. This component can be attributed to the residual elastic contribution due to the scattering from host-metal nuclei and, possibly, some trapped protons.

Since A_0 and Γ_2 appear to be nearly independent of Q, at the next stage of the analysis, these parameters have been fixed (being equal to their average values at a given temperature). Thus, only A_1 and Γ_1 remain as independent fit parameters. In this case, the fitting procedure becomes quite stable. The solid curve in figure 3 shows the fit of the three-component model (equation (1)) to the data, and the broken curves represent contributions of the different components.

QENS spectra for bm-$ZrCr_2H_3$ samples are qualitatively similar to those for cg-$ZrCr_2H_3$; they have been treated in the same way. For both bm-$ZrCr_2H_3$ (1 h) and bm-$ZrCr_2H_3$ (3 h), the three-component description becomes necessary at $T \geqslant 297$ K. This means that, for the ball-milled samples, the narrow Lorentzian component becomes visible at a higher temperature than for cg-$ZrCr_2H_3$ (250 K). The most pronounced difference between QENS spectra for the coarse-grained and ball-milled samples is related to the fraction of the elastic line intensity. This fraction, A_0, is found to be about 0.2 for bm-$ZrCr_2H_3$ (1 h) and about 0.3 for bm-$ZrCr_2H_3$ (3 h), i.e., considerably higher than for cg-$ZrCr_2H_3$($A_0 \approx 0.07$). The additional fraction of immobile protons in the ball-milled samples can be attributed to H atoms in the 'amorphous-like' regions. In fact, according to NMR data [21], the mobility of H atoms in these regions is much lower than in the C15-type phase. Therefore, on the time scale of our QENS experiments, H atoms in the amorphous-like regions are seen as immobile. It is interesting to note that comparison of the NMR data for the crystalline C15-type hydrides $ZrV_2H_x(D_x)$ and for the amorphous hydrides of identical compositions [31] has also revealed a significant reduction of the hydrogen mobility in the amorphous samples. The opposite trend in the H mobility for most of the amorphous hydrides studied and their crystalline counterparts [29] is usually attributed to the fact that a structural disorder may give rise to the opening of new 'easy paths' for H diffusion. On the other hand, for Laves-phase hydrides the diffusion barriers are originally quite low, so a structural disorder can only make the H diffusion more difficult.

3.3. Parameters of hydrogen motion: long-range diffusion

For cg-$ZrCr_2H_3$, the Q dependences of the half-width Γ_1 of the narrow quasielastic line, as derived from the QENS spectra measured at $T = 300$, 350, and 380 K, are shown in figure 4. For the measurements at other temperatures, the $\Gamma_1(Q)$ dependences have similar shapes. These shapes

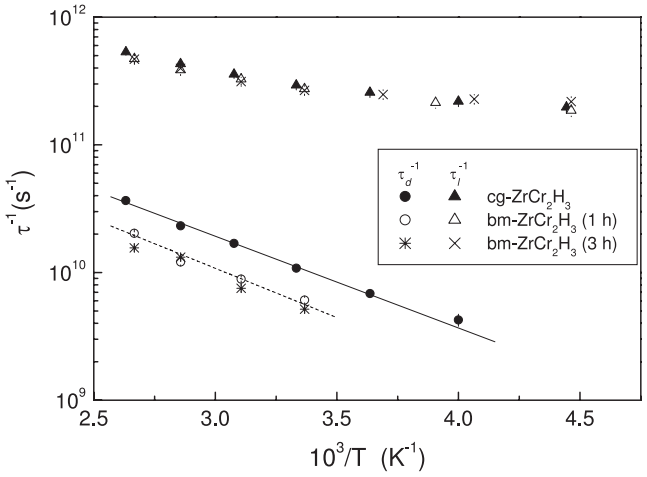

Figure 5. The hydrogen jump rates τ_d^{-1} and τ_l^{-1} in cg- and bm-$ZrCr_2H_3$ samples as functions of the inverse temperature. The full line shows the Arrhenius fit to the τ_d^{-1} data for cg-$ZrCr_2H_3$. The dashed line represents the Arrhenius fit to the τ_d^{-1} data for bm-$ZrCr_2H_3$ (1 h).

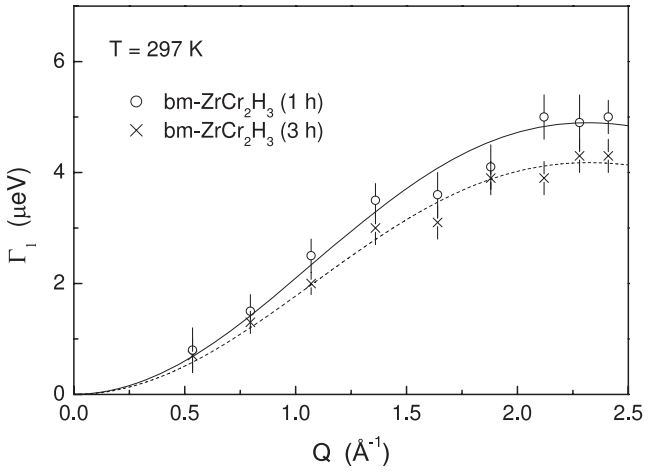

Figure 6. The HWHM of the narrow Lorentzian QENS component as a function of Q for bm-$ZrCr_2H_3$ (1 h) and bm-$ZrCr_2H_3$ (3 h) at $T = 297$ K. The full and dashed curves show the fits of the Chudley–Elliott model (equation (2)) to the data for the samples with $t_m = 1$ and 3 h, respectively.

are typical of the case of jump motion leading to long-range diffusion [6, 7]. For parametrization of the $\Gamma_1(Q)$ dependence, we have used the orientationally averaged Chudley–Elliott model [32]. The corresponding form of $\Gamma_1(Q)$ is

$$\Gamma_1(Q) = \frac{\hbar}{\tau_d}\left(1 - \frac{\sin QL}{QL}\right), \qquad (2)$$

where τ_d is the mean time between two successive H jumps leading to long-range diffusion, and L is the effective jump length. The fits of equation (2) to the data are shown by the solid curves in figure 4. The temperature dependence of the H jump rate τ_d^{-1} resulting from the Chudley–Elliott fits is presented in figure 5 by solid circles. This temperature dependence can be satisfactorily described by the Arrhenius law

$$\tau_d^{-1} = \tau_{d0}^{-1} \exp(-E_a^d/k_B T), \qquad (3)$$

where E_a^d is the activation energy for hydrogen diffusion. The solid line in figure 5 shows the Arrhenius fit to the τ_d^{-1} data for cg-$ZrCr_2H_3$; the corresponding fit parameters are $\tau_{d0}^{-1} = (2.8 \pm 0.4) \times 10^{12}$ s^{-1} and $E_a^d = 142 \pm 4$ meV. It should be noted that the value of E_a^d for cg-$ZrCr_2H_3$ is considerably higher than for the cg-$ZrCr_2H_x$ systems with low hydrogen concentrations (84 meV for $ZrCr_2H_{0.5}$, as found from NMR measurements [22], and 73 ± 3 meV for $ZrCr_2H_{0.45}$, from backscattering QENS experiments [20]). Thus, the activation energy for long-range H diffusion in $ZrCr_2H_x$ strongly increases with increasing hydrogen concentration. Since the lattice parameter of the C15-type $ZrCr_2H_x$ is known to grow substantially with increasing H content, these results support the idea [19] that the H jump rates (and the corresponding activation energies) in Laves-phase hydrides are very sensitive to changes in the distances between interstitial sites.

The values of L obtained from the Chudley–Elliott fits for cg-$ZrCr_2H_3$ are close to 2.0 Å at all the temperatures studied. These effective jump lengths are considerably longer than the distance r_2 between the nearest-neighbor g sites belonging to the adjacent hexagons (see figure 1). Indeed, the value of r_2 is 1.27, as derived from the neutron diffraction data on the positional parameters of D atoms occupying g sites in $ZrCr_2D_x$ [9, 11] and the actual lattice parameter of cg-$ZrCr_2H_3$. The fact that the effective jump lengths resulting from the Chudley–Elliott fits are considerably longer than r_2 appears to be common for a number of cubic Laves-phase hydrides [16, 18–20, 33]. This feature can be explained [16, 20] in terms of the model of H motion with two frequency scales: the rate τ_l^{-1} of jumps within the g site hexagons and the rate τ_d^{-1} of jumps between the adjacent hexagons, $\tau_d^{-1} \ll \tau_l^{-1}$. Such a model implies [16, 20] that τ_d is the mean residence time of a hydrogen atom at a g site hexagon (not at a single interstitial site, as is commonly assumed). Since a hydrogen atom may enter a g site hexagon through one site and leave it via another site, the total displacement for the time τ_d is the distance between the nearest g sites at the adjacent hexagons plus the additional displacement between the initial and final positions of a hydrogen atom at the hexagon. The half-width Γ_1 is determined by the slower frequency scale τ_d^{-1}; therefore, the apparent jump length L derived from the Q dependence of Γ_1 would be larger than the distances between the nearest-neighbor interstitial sites. More precisely, we expect a certain distribution of L values ranging from $r_2 = 1.27$ Å to ∼3.1 Å (the distance between a g site and the farthest g site at the adjacent hexagon). Hence, the average value $L \approx 2.0$ Å derived from the Chudley–Elliott analysis seems to be reasonable.

For the ball-milled $ZrCr_2H_3$ samples, the Q dependences of Γ_1 resemble those for coarse-grained $ZrCr_2H_3$. As an example of the data, figure 6 shows the Q dependences of Γ_1 for bm-$ZrCr_2H_3$ (1 h) and bm-$ZrCr_2H_3$ (3 h) at $T = 297$ K. For both ball-milled samples, these dependences can be satisfactorily described by the Chudley–Elliott model

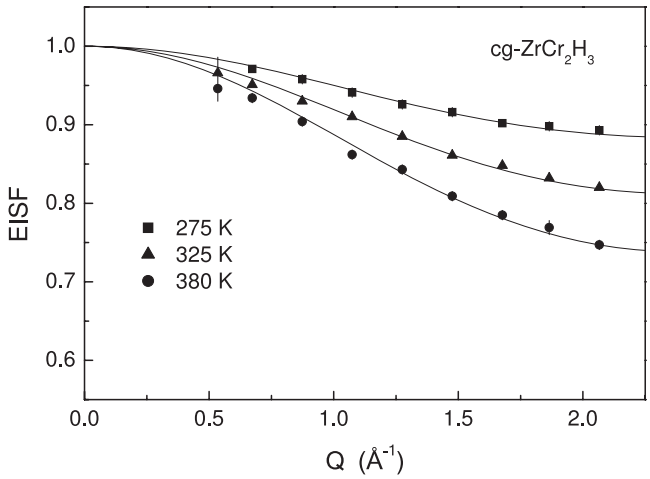

Figure 7. The elastic incoherent structure factor for the hydrogen sublattice in cg-$ZrCr_2H_3$ as a function of Q at $T = 275$, 325, and 375 K. The full curves show the fits of the six site model (equation (4)) with fixed $r = 1.18$ Å to the data.

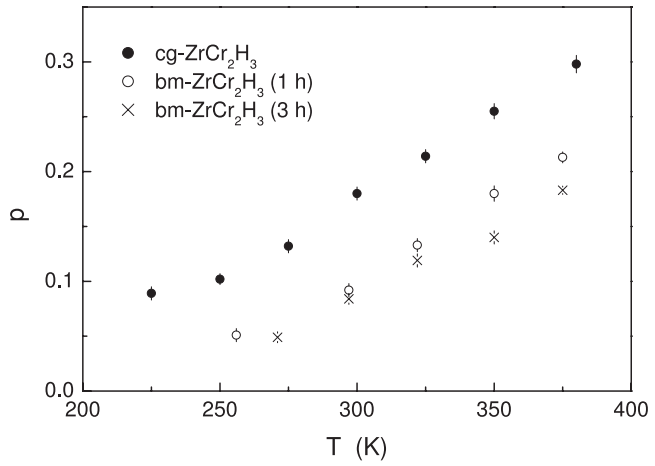

Figure 8. The temperature dependence of the fraction of H atoms in C15-type grains participating in the fast localized motion for cg-$ZrCr_2H_3$, bm-$ZrCr_2H_3$ (1 h), and bm-$ZrCr_2H_3$ (3 h).

(the dashed and solid curves in figure 6 for $t_m = 1$ h and 3 h, respectively). The values of τ_d^{-1} resulting from the Chudley–Elliott fits for the ball-milled samples are included in figure 5. As can be seen from this figure, the jump rates τ_d^{-1} for the ball-milled samples are lower than for the coarse-grained sample. Thus, lattice distortions in the C15-type grains of the ball-milled samples lead to the decrease in H mobility in these grains. For a qualitative interpretation of such a decrease, one may use the same arguments as in the case of H mobility in the 'amorphous-like' regions (see section 3.2). The dashed line in figure 5 shows the Arrhenius fit to the τ_d^{-1} data for bm-$ZrCr_2H_3$ (1 h); the corresponding fit parameters are $\tau_{d0}^{-1} = (2.2 \pm 0.5) \times 10^{12}$ s^{-1} and $E_a^d = 153 \pm 6$ meV. As in the case of cg-$ZrCr_2H_3$, the values of L derived from the Chudley–Elliott fits for both bm-$ZrCr_2H_3$ samples are close to 2.0 Å at all the temperatures studied. These results suggest that the microscopic picture of H jump motion in the C15-type grains of the bm-$ZrCr_2H_3$ remains the same as in the coarse-grained material.

3.4. Localized hydrogen motion

In this section, we shall focus on the behavior of the broad quasielastic component related to the localized H motion. The geometry of the localized H motion is expected to determine the Q dependence of the elastic incoherent structure factor (EISF) [6, 7]. For QENS spectra described by equation (1), the 'resolution-limited' EISF is defined as $(A_0 + A_1)/(A_0 + A_1 + A_2) = A_0 + A_1$. Assuming that the purely elastic component of these QENS spectra is dominated by the host-metal contribution (for cg-$ZrCr_2H_3$) or by the same contribution and the contribution due to H atoms in the amorphous-like regions (for the bm-$ZrCr_2H_3$ samples), we can conclude that the EISF for the hydrogen sublattice in C15-type grains is given by the ratio $A_1/(A_1 + A_2)$. The Q dependences of the EISF for the H sublattice in cg-$ZrCr_2H_3$ at several temperatures are shown in figure 7. It can be seen that the measured EISF is temperature dependent, decreasing with increasing T. This feature is common to all the Laves-phase hydrides studied [16–20, 34]. In order to account for this feature, we have to assume that only a fraction p of the H atoms participate in the fast localized motion, and the fraction increases with temperature. The existence of a fraction $1 - p$ of 'immobile' protons (on the frequency scale of τ_1^{-1}) is expected to originate from the H–H interaction leading to the formation of some ordered atomic configurations at low temperatures [16]. For example, two H atoms occupying g sites on the same hexagon may block the localized motion over this hexagon. As the temperature increases, such ordered configurations should be progressively destroyed by thermal fluctuations; this results in the observed growth of p with increasing T.

Taking into account the fraction p, the orientationally averaged form of the EISF for the model of localized motion over a regular hexagon with the nearest-neighbor intersite distance r [6, 7] can be written as

$$\mathrm{EISF} = 1 - p + \frac{p}{6}[1 + 2j_0(Qr) + 2j_0(Qr\sqrt{3}) + j_0(2Qr)], \quad (4)$$

where $j_0(x)$ is the spherical Bessel function of zeroth order. We have found that equation (4) satisfactorily describes the experimental Q dependences of the EISF for cg-$ZrCr_2H_3$. The fit of equation (4) to the measured Q dependence of the EISF at 380 K yields $p = 0.285 \pm 0.008$ and $r = 1.23 \pm 0.05$ Å. The fitted r value is close to the nearest-neighbor g–g distance in the g site hexagon, $r_1 = 1.18$ Å, as derived from the structure [9, 11] of $ZrCr_2H_3$. Thus, the observed Q dependence of the EISF for cg-$ZrCr_2H_3$ is consistent with the localized H motion over g site hexagons. By fixing the value of r to $r_1 = 1.18$ Å, we have found reasonable fits of the six site model (equation (4)) to the data at all temperatures in the range studied with p as the only fit parameter. These fits are shown by solid lines in figure 7. The temperature dependence of p resulting from these fits is shown in figure 8 by solid circles. As can be seen from figure 8, the fraction p in cg-$ZrCr_2H_3$ increases by nearly a factor of three in the range

225–380 K. However, we could not satisfactorily describe the temperature dependence of p for cg-$ZrCr_2H_3$ in terms of the usual approach [35] based on the assumption of a certain energy gap between 'immobile' and mobile H states. It should be noted that the values of p for cg-$ZrCr_2H_3$ are considerably smaller than those found for $ZrCr_2H_{0.45}$ [20]. This supports the idea that the fraction $1 - p$ of 'immobile' protons originate from H–H interactions.

The jump rate of the localized H motion, τ_1^{-1}, should be proportional to the half-width of the broad quasielastic component. A rigorous description in terms of the six site model [6] suggests that this quasielastic component is a sum of three Lorentzian lines with the half-widths $0.5\hbar\tau_1^{-1}$, $1.5\hbar\tau_1^{-1}$ and $2\hbar\tau_1^{-1}$, and Q-dependent amplitudes. However, as has been noted previously [16, 36], because of the limited experimental accuracy, it is difficult to distinguish between such a three-component quasielastic line and a single Lorentzian with a width independent of Q in the case of a rather weak quasielastic line coexisting with a strong elastic one. We have adopted the simplified description based on a single Lorentzian with $\Gamma_2 \approx 0.55\hbar\tau_1^{-1}$ [6]; such a description is very close to the rigorous one at $Qr \leqslant 1.5$ [6]. The jump rates τ_1^{-1} derived from the measured half-widths Γ_2 for cg-$ZrCr_2H_3$ are included in figure 5 (solid triangles). As can be seen from this figure, the temperature dependence of τ_1^{-1} is considerably weaker than that of τ_d^{-1}; moreover, $\tau_1^{-1}(T)$ deviates from Arrhenius behavior. Both these features are typical of the localized H motion in Laves-phase hydrides [19, 34, 37]. At room temperature, the jump rate τ_1^{-1} for cg-$ZrCr_2H_3$ is a factor of 27 higher than τ_d^{-1}. Such a value of τ_d/τ_1 is consistent with a rather small difference between r_2 and r_1 for $ZrCr_2H_x$ ($r_2/r_1 \approx 1.08$). For comparison, for the C15-type hydride TaV_2H_x with $r_2/r_1 = 1.45$, the ratio τ_d/τ_1 at 300 K exceeds 10^3 [19].

For the bm-$ZrCr_2H_3$ samples, the behavior of the EISF for the H sublattice in C15-type grains resembles that for the coarse-grained sample. As an example of the data, figure 9 shows the Q dependences of the EISF at 375 K for bm-$ZrCr_2H_3$ (1 h) and bm-$ZrCr_2H_3$ (3 h). For the sample with $t_m = 3$ h, the data obtained at two values of the incident neutron wavelength (4.8 and 6.0 Å) are shown; they appear to be close to each other. Comparison of figures 7 and 9 indicates that, for the ball-milled samples, the range of the EISF variation is smaller than for the coarse-grained sample at nearly the same temperature. This suggests that the values of p for the bm-$ZrCr_2H_3$ samples are smaller than for cg-$ZrCr_2H_3$. For parametrization of the EISF data for the ball-milled samples, we used the six site model (equation (4)) with r fixed to $r_1 = 1.18$ Å. The corresponding fits are shown by solid lines in figure 9. Reasonable fits of this model to the data have also been found at the other temperatures studied. The values of p resulting from the fits for the ball-milled samples are included in figure 8. As can be seen from this figure, the results of the fits support our qualitative conclusion that ball milling leads to the decrease in the fraction of H atoms participating in the fast localized motion in C15-type grains. Such a decrease can be attributed to lattice distortions induced by ball milling. In fact, the lattice distortions should also distort at least some of the g site hexagons, making them unsuitable for the fast localized H motion.

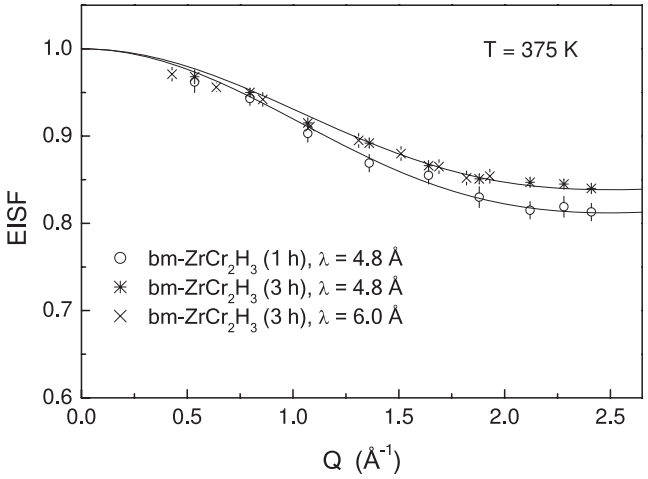

Figure 9. The Q dependence of the elastic incoherent structure factor for the hydrogen sublattice in C15-type grains for the bm-$ZrCr_2H_3$ samples at $T = 375$ K. For bm-$ZrCr_2H_3$ (3 h), the results obtained from the measurements at both $\lambda = 4.8$ and 6.0 Å are shown. The full curves represent the fits of the six site model (equation (4)) with fixed $r = 1.18$ Å to the data.

The jump rates of the localized H motion in C15-type grains of the ball-milled samples have been obtained from the half-widths Γ_2 of the broad quasielastic component in the same way as for the coarse-grained sample. The corresponding values of τ_1^{-1} for the bm-$ZrCr_2H_3$ are included in figure 5. In contrast to τ_d^{-1}, the jump rates τ_1^{-1} for the ball-milled samples appear to be close to those for cg-$ZrCr_2H_3$. However, we cannot exclude a possibility of a certain distribution of τ_1^{-1} values in the nanostructured samples.

4. Conclusions

The analysis of our quasielastic neutron scattering data for coarse-grained C15-type $ZrCr_2H_3$ has shown that the diffusive motion of hydrogen in this system can be described in terms of at least two jump processes with different characteristic frequencies. The faster process with the jump rate τ_1^{-1} corresponds to localized H motion over the hexagons formed by interstitial g sites, and the slower process with the jump rate τ_d^{-1} is associated with H jumps leading to long-range diffusion. The ratio of the jump rates for these two processes, τ_d/τ_1, is found to be about 27 at 300 K. The temperature dependence of τ_d^{-1} for coarse-grained $ZrCr_2H_3$ in the range 250–380 K can be reasonably well described by the Arrhenius law with the activation energy $E_a^d = 142 \pm 4$ meV. In the same range, the temperature dependence of τ_1^{-1} deviates from Arrhenius behavior, being considerably weaker than that of τ_d^{-1}.

The ball-milled $ZrCr_2H_3$ samples are characterized by a coexistence of the C15-type grains (with an average size of 20 nm or less) and the strongly distorted (amorphous-like) regions, the fraction of which increases with the milling time. H atoms in the strongly distorted regions give a very broad

contribution to the low-temperature vibrational spectrum of hydrogen; these atoms are found to be immobile on the time scale of our QENS experiments. The microscopic picture of H jump motion in the C15-type grains of the nanostructured samples is similar to that in coarse-grained $ZrCr_2H_3$. However, the ball milling is found to lead to a considerable decrease in the jump rate τ_d^{-1} and to an increase in the associated activation energy E_a^d. Another pronounced effect of ball milling is the drop of the fraction of H atoms participating in the fast localized motion in the C15-type grains. This effect can be related to lattice defects appearing in the course of ball milling.

Acknowledgments

This work utilized facilities supported in part by the National Science Foundation under Agreement No. DMR-0454672. This work was also supported by the Priority Program 'Basics of Development of Energy Systems and Technologies' of the Russian Academy of Sciences. AVS acknowledges financial support from the NIST Center for Neutron Research.

References

[1] Zaluska A, Zaluski L and Ström-Olsen J O 1999 *J. Alloys Compounds* **288** 217
[2] Huot J, Liang G and Schulz R 2001 *Appl. Phys.* A **72** 187
[3] Barkhordarian G, Klassen T and Bormann R 2004 *J. Alloys Compounds* **364** 242
[4] Yermakov A Ye, Mushnikov N V, Uimin M A, Gaviko V S, Tankeyev A P, Skripov A V, Soloninin A V and Buzlukov A L 2006 *J. Alloys Compounds* **425** 367
[5] Barnes R G 1997 *Hydrogen in Metals III* ed H Wipf (Berlin: Springer) p 93
[6] Bée M 1988 *Quasielastic Neutron Scattering* (Bristol: Hilger)
[7] Hempelmann R 2000 *Quasielastic Neutron Scattering and Solid State Diffusion* (Oxford: Clarendon)
[8] Shaltiel D, Jacob I and Davidov D 1977 *J. Less-Common Met.* **53** 117
[9] Fruchart D, Rouault A, Shoemaker C B and Shoemaker D P 1980 *J. Less-Common Met.* **73** 363
[10] Irodova A V, Lavrova O A, Laskova G V and Padurets L N 1982 *Sov. Phys.—Solid State* **24** 22
[11] Kohlmann H, Fauth F and Yvon K 1999 *J. Alloys Compounds* **285** 204
[12] Irodova A V and Suard E 2000 *J. Alloys Compounds* **299** 32
[13] Renz W, Majer G, Skripov A V and Seeger A 1994 *J. Phys.: Condens. Matter* **6** 6367
[14] Bowman R C, Craft B D, Attalla A and Johnson J R 1983 *Int. J. Hydrog. Energy* **8** 801
[15] Skripov A V, Rychkova S V, Belyaev M Yu and Stepanov A P 1990 *J. Phys.: Condens. Matter* **2** 7195
[16] Skripov A V, Cook J C, Sibirtsev D S, Karmonik C and Hempelmann R 1998 *J. Phys.: Condens. Matter* **10** 1787
[17] Skripov A V, Cook J C, Udovic T J and Kozhanov V N 2000 *Phys. Rev.* B **62** 14099
[18] Bull D J, Broom D P and Ross D K 2003 *Chem. Phys.* **292** 153
[19] Skripov A V 2003 *Defect Diffus. Forum* **224/225** 75
[20] Skripov A V, Pionke M, Randl O and Hempelmann R 1999 *J. Phys.: Condens. Matter* **11** 1489
[21] Soloninin A V, Buzlukov A L, Skripov A V, Aleksashin B A, Tankeyev A P, Yermakov A Ye, Mushnikov N V, Uimin M A and Gaviko V S 2008 *J. Phys.: Condens. Matter* **20** 275239
[22] Skripov A V and Belyaev M Yu 1993 *J. Phys.: Condens. Matter* **5** 4767
[23] Stoddard R D and Conradi M S 1998 *Phys. Rev.* B **57** 10455
[24] Udovic T J *et al* 2008 *Nucl. Instrum. Methods* A **588** 406
[25] Copley J R D and Cook J C 2003 *Chem. Phys.* **292** 477
[26] Copley J R D and Udovic T J 1993 *J. Res. Natl Inst. Stand. Technol.* **98** 71
[27] Fernandez J F, Kemali M, Ross D K and Sanchez S 1999 *J. Phys.: Condens. Matter* **11** 10353
[28] Skripov A V, Natter H and Hempelmann R 2001 *Solid State Commun.* **120** 265
[29] Richter D, Hempelmann R and Bowman R C 1992 *Hydrogen in Intermetallic Compounds II* ed L Schlapbach (Berlin: Springer) p 97
[30] Ross D K 1997 *Hydrogen in Metals III* ed H Wipf (Berlin: Springer) p 153
[31] Rychkova S V, Belyaev M Yu, Skripov A V and Stepanov A P 1988 *Sov. Phys.—Solid State* **30** 1285
[32] Chudley C T and Elliott R J 1961 *Proc. Phys. Soc.* **77** 353
[33] Campbell S I, Kemali M, Ross D K, Bull D J, Fernandez J F and Johnson M R 1999 *J. Alloys Compounds* **293–295** 351
[34] Skripov A V, Udovic T J and Rush J J 2007 *Phys. Rev.* B **76** 104305
[35] Berk N F, Rush J J, Udovic T J and Anderson I S 1991 *J. Less-Common Met.* **172–174** 496
[36] Schönfeld C, Hempelmann R, Richter D, Springer T, Dianoux A J, Rush J J, Udovic T J and Bennington S M 1994 *Phys. Rev.* B **50** 853
[37] Skripov A V, Gonzalez M A and Hempelmann R 2008 *J. Phys.: Condens. Matter* **20** 085213